Screen-Printed Potassium-Selective Organic Electrochemical Transistors: Electrical and Electrochemical Investigation of Ion-Sensing Mechanisms

Fahian Mahmud[1], Alejandro Bello[1], Ashok Kumar[2], Abner Renteria[3], Abijeet Singh Mehta[3], Vinay Budhraja[1*]

[1]Department of Electrical Engineering, Northern Illinois University, DeKalb IL, USA
[2]Department of Applied Sciences, National Institute of Technical Teachers' Training and Research Chandigarh, Chandigarh, India
[3]Department of Health and Biomedical Sciences, University of Texas Rio Grande Valley, TX, USA

E-mail: vbudhraja@niu.edu

Keywords: Organic electrochemical transistor, potassium sensor, sensor, electrochemical sensor, PEDOT:PSS, potassium ion-selective membrane, ionophore

Abstract:

Potassium-selective organic electrochemical transistors (OECTs) provide a route for coupling ion recognition with amplified electronic readout in low-voltage sensing platforms. Here, we report a multilayer screen-printed OECT incorporating Ag/AgCl contacts, carbon conductors, a polyethylene glycol (PEG)- and Tween 80-modified PEDOT:PSS channel, dielectric encapsulation, and a potassium ionophore III-based ion-selective membrane. The electrical and electrochemical response of the device was investigated over KCl concentrations from 1.0×10^{-4} to 1.67 M using output and transfer characteristics, transient gate modulation, cyclic voltammetry, electrochemical impedance spectroscopy, and interference measurements. Increasing K^+ concentration produced progressively stronger drain-current modulation, yielding a current sensitivity of 4.61 μA decade^{-1} ($R^2 = 0.9918$) and an equivalent gate-voltage-shift sensitivity of 137.7 mV decade^{-1} ($R^2 = 0.9953$). Transient measurements showed reversible and concentration-dependent switching, while cyclic voltammetry revealed increasing anodic and cathodic current magnitudes with increasing KCl concentration. Impedance spectroscopy further showed a concentration-dependent reduction in effective electrochemical impedance and enhanced low-frequency capacitive behavior. The device exhibited preferential response to K^+ over NH_4^+, Na^+, Mg^{2+}, and Ca^{2+}, with drain-current modulation approximately 1.3–4.8 times larger than that of the tested interferents. The combined measurements establish a direct relationship between selective K^+ transport, interfacial electrochemical processes, and modulation of electronic conduction in the PEDOT:PSS channel, providing mechanistic insight into ion sensing in screen-printed OECTs.

1. Introduction

Potassium ions (K^+) are essential to physiological homeostasis and plant nutrition. In humans, K^+ is the principal intracellular cation and governs membrane potential, neuromuscular signaling, muscle contraction, and fluid balance [1]. As a result, potassium imbalance carries direct clinical

significance. Localized K^+ dynamics can also carry organ-specific information: K^+-rich endolymph, for example, is central to sensory transduction in the cochlea which has motivated miniaturized sensors for continuous monitoring in the inner ear [2]. Sweat offers a less invasive route for tracking electrolyte loss during exercise, and wearable systems have combined K^+ detection with glucose or sodium measurement to assess hydration and physiological status [3], [4]. In agriculture, K^+ regulates osmotic balance, stomatal function, enzyme activation, and photosynthesis [5] and in-soil K^+ probes have accordingly been investigated for monitoring nutrient availability at multiple depths [6]. Across these applications, sensors must remain selective and reliable over markedly different concentration ranges, ionic backgrounds, sample volumes, and operating environments.

Potassium is commonly measured using ion-selective electrodes (ISEs), potentiometric cells, and ion-sensitive field-effect transistors. In a conventional K^+-ISE, a plasticized polymer membrane containing a selective ionophore and lipophilic ionic sites develops an interfacial potential that depends on K^+ activity. Solid-contact architectures remove the internal filling solution and support miniaturization, wearability, and point-of-care use [7]. Polymeric K^+-selective membranes have been integrated into digital microfluidic platforms [8], laser-induced graphene electrodes for salivary analysis [9], and wearable sweat systems [3], [4]. However, potentiometric sensors produce a voltage without intrinsic gain and require a stable reference electrode and high-input-impedance instrumentation. Their logarithmic response also makes small concentration differences difficult to resolve in samples with a high background electrolyte, such as potassium determination in serum containing a much larger sodium concentration [10].

Organic electrochemical transistors (OECTs) address these limitations because they operate at low voltages and couple ionic transport in an electrolyte to electronic conduction in an organic mixed ionic-electronic conductor [11]. The concept originated with the electrolyte-gated polypyrrole transistor reported by White et al. in 1984, in which three closely spaced gold microelectrodes coated with polypyrrole were controlled by a small gate charge that shifted the oxidation state and conductivity of the polymer [12]. Modern depletion-mode PEDOT:PSS OECTs operate through the same electrochemical principle: a positive gate bias drives cations into the channel, compensating the sulfonate groups and reducing the population of oxidized PEDOT charge carriers, thereby decreasing the drain current [11], [13]. Because the ionic charge is stored throughout the channel volume rather than at a single interface, as in a conventional field-effect transistor, transconductance scales with the channel geometry Wd/L and the material parameter μC^*, where μ is the electronic mobility and C^* is the volumetric capacitance [14]. This volumetric coupling enables millisiemens-scale transconductance in microscale devices, but it also means that increasing channel thickness increases ionic charging time, creating a trade-off between signal amplification and response speed [11], [13]. PEDOT:PSS is especially attractive for printed OECTs because it is commercially available as an aqueous dispersion and compatible with additive, low-temperature fabrication on diverse substrates. This relevance to implantable bioelectronics was also discussed from an electron-device and systems-roadmap perspective by Mahmud et al.[15] .

The gate/electrolyte and electrolyte/channel interfaces determine how the applied gate bias is distributed within an OECT. For effective channel modulation with a polarizable gate, the gate capacitance should be substantially larger than the channel capacitance, whereas a nonpolarizable Ag/AgCl gate minimizes the voltage drop at the gate/electrolyte interface [13], [14]. Analyte-dependent Faradaic reactions can further shift the effective gate voltage in an early enzymatic OECT glucose sensor, Bernards et al. related this shift to the Nernstian change in interfacial

potential and showed that the response scaled with the gate-to-channel capacitance ratio [16]. Ion selectivity is commonly introduced by coupling the OECT to an ion-selective membrane (ISM), either at the gate, directly on the channel, or through an intermediate ionic element. Early K^+-selective OECTs demonstrated that the transconductance of the transistor could convert an ionophore-generated membrane potential into a current sensitivity approaching 50 μA decade^{-1} [17]. Subsequent studies expanded the device format and target application. Textile OECTs enabled wearable K^+ monitoring in sweat [18]; ion-selective OECTs were developed for sodium analysis in blood [19]; and microfabricated OECT arrays functionalized with different ISMs enabled real-time multiplexed monitoring of Na^+ and K^+ [20]. A paper-based thick-film IS-OECT optimized for clinical potassium analysis reported a 0.1-100 mM linear range and discrimination of 0.05 mM concentration changes in artificial serum [10]. More recently, floating-gate OECT circuits spatially separated the selective membrane from channel modulation and detected K^+ in the presence of a substantially higher Na^+ background [21], while paper-based IS-OECTs have been extended to combined potassium and creatinine determination [22]. Of particular relevance to scalable fabrication, Strand et al. reported fully screen-printed K^+-selective OECTs on flexible polyethylene naphthalate for whole-plant sap analysis. Incorporating 25 wt% sorbitol into the PEDOT:PSS formulation increased the maximum transconductance from 2.4 to 5.0 mS, while the completed sensors achieved current and voltage sensitivities of 170 μA decade^{-1} and 99 mV decade^{-1}, respectively, a 10 μM detection limit, and analysis of a single drop of raw sap within 3 min [23]. Most recently, a flexible three-channel OECT array with a shared gate simultaneously detected Na^+, K^+, and Ca^{2+} in human biofluids, with sensitivity exceeding 1 mA decade^{-1} and a K^+ detection limit of 4.92 μM; its miniaturized wireless readout and machine-learning workflow further addressed cross-interference and enabled mobile, real-time physiological monitoring [24].

Collectively, these studies establish the versatility of OECT-based ion sensing and confirm that fully printed K^+-selective transistors are feasible. Nevertheless, the relationship between K^+ concentration and the transistor, switching, and interfacial electrochemical behavior of a multilayer screen-printed Ag/AgCl–carbon–PEDOT:PSS platform remains insufficiently resolved. Prior studies have generally emphasized analytical calibration, selectivity, or system-level signal processing rather than examining the same printed device through output and transfer characteristics, dynamic gate switching, cyclic voltammetry, and electrochemical impedance spectroscopy together. Such a combined analysis can connect amplified drain-current changes with concentration-dependent ion transport, charge transfer, and interfacial capacitance, while the multilayer process itself can pattern contacts, carbon conductors, the organic channel, and dielectric encapsulation by scalable additive manufacturing.

Our previous work established the electrochemical transport, transconductance, gate leakage, and parasitic effects of unfunctionalized screen-printed PEDOT:PSS OECTs [25]. The present study extends this platform to selective ion sensing by integrating a potassium ionophore III-based ion-selective membrane with a multilayer screen-printed Ag/AgCl–carbon–PEDOT:PSS architecture. The key contribution is a systematic electrical and electrochemical investigation of K^+-dependent transduction using complementary output and transfer characteristics, transient gate modulation, cyclic voltammetry, electrochemical impedance spectroscopy, and interference measurements. By correlating these responses within the same device architecture, the study examines how K^+-dependent ion transport and interfacial electrochemical processes influence modulation of the PEDOT:PSS channel.

Here, the potassium-selective OECT is evaluated over KCl concentrations ranging from 1.0×10^{-4} to 1.67 M. Electrical measurements quantify concentration-dependent drain-current

modulation and equivalent gate-voltage shifts, while transient measurements probe dynamic ionic modulation and switching behavior. Cyclic voltammetry and electrochemical impedance spectroscopy provide complementary information on electrochemical charging, ion transport, interfacial polarization, and impedance changes, and interference measurements assess the preferential response to K^+ relative to NH_4^+, Na^+, Mg^{2+}, and Ca^{2+}. Together, these measurements establish relationships between selective ion transport, interfacial electrochemistry, and electronic modulation in a scalable screen-printed OECT architecture.

2. Experimental Details

2.1. Materials

The organic semiconductor poly(3,4-ethylenedioxythiophene)(styrene sulfonate) (PEDOT:PSS, Clevios™), Ag/AgCl conductive ink, carbon conductive ink, and dielectric encapsulation ink were used for device fabrication. Potassium ion-selective membranes (K^+-ISM) were prepared using high-molecular-weight poly(vinyl chloride) (PVC), potassium ionophore III, potassium tetrakis(4-chlorophenyl) borate (KTpClPB), and 2-nitrophenyl octyl ether (2-NPOE) dissolved in tetrahydrofuran (THF). Potassium chloride (KCl), sodium chloride (NaCl), and deionized (DI) water were used for sensor conditioning and electrical characterization.

2.2 Potassium Ion-Selective Membrane Preparation

The potassium ion-selective membrane (K^+-ISM) solution was prepared by dissolving poly(vinyl chloride) (PVC, 32.80 wt%), 2-nitrophenyl octyl ether (2-NPOE, 65 wt%), potassium ionophore III (2 wt%), and potassium tetrakis(4-chlorophenyl) borate (KTpClPB, 0.2 wt%) in tetrahydrofuran (THF). The solution was continuously stirred until a homogeneous membrane precursor was obtained. The resulting membrane solution was used for drop-casting onto the transistor sensing region.

2.3 Device Fabrication

The potassium-selective OECT was fabricated using a multilayer screen-printing process, as illustrated in Figure 1. Ag/AgCl electrodes defining the source, drain, gate, and auxiliary contact pads were first screen-printed and thermally cured, after which a carbon layer was printed on top of the Ag/AgCl electrodes to improve electrical conductivity and provide a stable interface for the active sensing layers.

A PEDOT:PSS channel was subsequently screen-printed between the source and drain electrodes and thermally annealed at 120°C for 30 minutes to form the organic semiconducting channel. Before printing, the PEDOT:PSS paste was modified by incorporating 3 wt.% polyethylene glycol (PEG) and 0.67 wt.% Tween 80. PEDOT:PSS is a p-type, hole-conducting organic semiconductor that supports mixed ionic and electronic transport, making it well suited for organic electrochemical transistor applications [26], and the addition of PEG and Tween 80 improves the printability, electrical conductivity, and stability of the channel, thereby enhancing overall device performance [27], [28].

Following channel deposition, a dielectric encapsulation layer was printed to electrically isolate the conductive tracks while exposing only the active channel and gate regions. The structure of regular OECTs have shown stable performance at two different channel lengths [25]. The fabricated devices were then immersed in 0.1 M NaCl solution for 1 h to condition the PEDOT:PSS

channel. An ion-treatment step using NaCl introduces mobile ions into the bulk of the composite layer, thereby forming an internal ionic reservoir within the channel [23], [29].

After conditioning, the potassium ion-selective membrane was drop-cast over the exposed channel region and allowed to dry under ambient conditions. Finally, a polydimethylsiloxane (PDMS) reservoir was attached to the device surface to confine the electrolyte during electrical and electrochemical measurements.

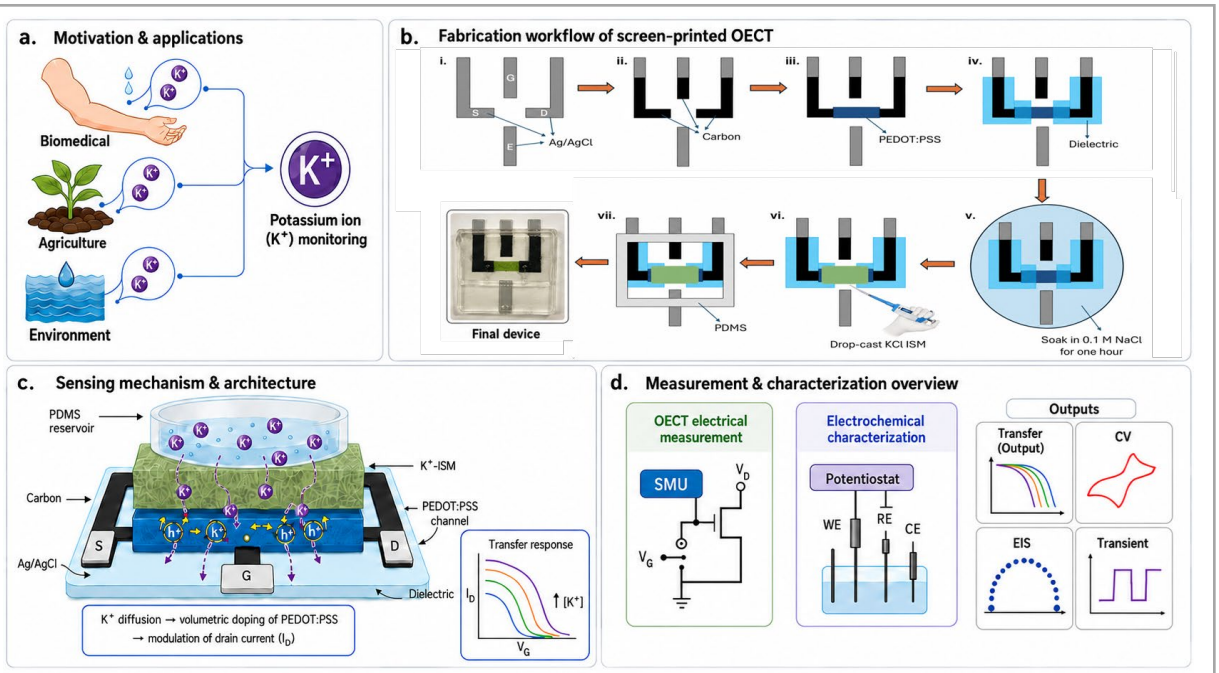


Figure 1. Overview of the screen-printed potassium-selective organic electrochemical transistor (OECT) platform. **(a)** Motivation and potential applications of K^+ monitoring in biomedical, agricultural, and environmental settings. **(b)** Multilayer fabrication workflow of the screen-printed OECT **(c)** Schematic of the device architecture and proposed K^+-sensing mechanism, illustrating selective K^+ transport **(d)** Electrical and electrochemical characterization scheme, including OECT transfer/output and transient measurements, cyclic voltammetry (CV), and electrochemical impedance spectroscopy (EIS).

2.4 Morphological and Elemental Characterization

The surface morphology of the individual printed layers, including Ag/AgCl, carbon, PEDOT, and potassium ion-selective membrane films, was investigated using scanning electron microscopy (SEM) as shown in figure 2. Cross-sectional interface regions between the Ag/AgCl-carbon, carbon-PEDOT, and K^+-ISM-carbon layers were also examined to evaluate film uniformity, surface coverage, and interfacial continuity. The Ag/AgCl layer exhibited a porous, granular morphology that increases electrochemically active surface area and facilitates ion exchange, while the printed carbon layer showed a rough, interconnected microstructure that provides efficient electrical pathways and enhanced adhesion between successive layers.

The PEDOT:PSS film displayed a relatively uniform morphology with interconnected polymer domains, favorable for charge transport and volumetric ion penetration during transistor operation,

and the potassium ion-selective membrane exhibited a dense, continuous structure indicating successful membrane formation over the sensing region.

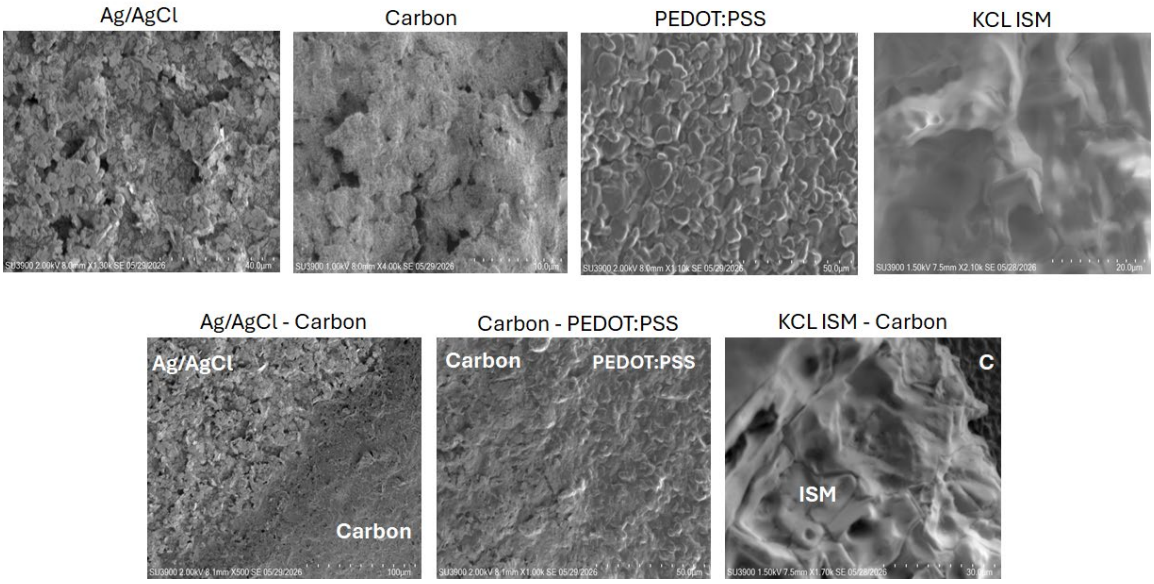


Figure 2. SEM images of individual printed layers (Ag/AgCl, carbon, PEDOT:PSS, and K^+-ISM) and interface regions including Ag/AgCl–carbon, carbon–PEDOT:PSS, and K^+-ISM–carbon.

SEM images further demonstrated strong interfacial continuity between Ag/AgCl and carbon layers, as well as between carbon and PEDOT:PSS. The PEDOT:PSS film appeared rougher after polyethylene glycol and tween80 modification, increasing the effective surface area and facilitating ionic transport[27], [30], [31] . The K^+-ISM/carbon interface showed conformal membrane coverage without significant cracks or delamination. Such structural integrity is critical for stable ion transport and reproducible sensor performance. The observed multilayer morphology confirms the compatibility of screen printing for scalable fabrication of potassium-selective OECT devices.

The elemental composition of the potassium ion-selective membrane was analyzed using energy-dispersive X-ray spectroscopy (EDS) (Figure S1). The spectrum exhibits prominent peaks corresponding to carbon (C), oxygen (O), chlorine (Cl), and potassium (K), confirming presence of the membrane constituents. Carbon and oxygen originate primarily from the PVC polymer matrix and plasticizer (2-NPOE), while chlorine is associated with the PVC backbone and potassium tetrakis(4-chlorophenyl) borate (KTpClPB).

Quantitative analysis revealed elemental compositions of approximately 67.6 wt% C, 21.9 wt% Cl, 7.5 wt% O, 1.5 wt% N and 1.4 wt% K demonstrating a chemically stable ion-selective layer. The successful incorporation of potassium-containing species is essential for selective ion transport and efficient modulation of the OECT channel.

2.5 Electrical and Electrochemical Characterization

The electrical and electrochemical characterization of the OECT devices was performed according to the guidelines reported by Ohayon et. al.[32]. Electrical measurements of the

potassium-selective OECT were conducted using a Keithley 4200 semiconductor parameter analyzer. Output characteristics were recorded by sweeping the drain–source voltage (V_{DS}) from 0 to -1.5 V at different gate–source voltages (V_{GS}) from 0 to 1 V. Transfer characteristics were obtained by sweeping V_{GS} from 0 to 1 V at fixed V_{DS} value at -2 V in potassium chloride solutions with varying concentrations.

Sensing performance was evaluated using KCl concentrations ranging from 0.0001 M to 1.67 M. For each measurement, the electrolyte solution was introduced into the PDMS reservoir covering both the gate and channel regions. The variation in drain current with potassium concentration was used to construct calibration curves and determine sensor sensitivity.

Electrochemical characterization was carried out using a PalmSens potentiostat. Cyclic voltammetry (CV) measurements were performed in the same KCl solutions, from 0.0001 M to 1.67 M, to evaluate the electrochemical activity of the sensing interface: the potential was swept within a fixed voltage window at a constant scan rate of 50 mV/s, and the resulting oxidation and reduction currents were recorded.

Electrochemical impedance spectroscopy (EIS) measurements were conducted over a frequency range from 10 Hz to 100 kHz using a sinusoidal excitation signal. following the procedure described by Luginieski et. al. [33]. During the measurements, the drain and source terminals were short-circuited, the DC bias was held at 0.20 V, and an AC amplitude of 0.05 V was applied. Nyquist and Bode plots were analyzed to evaluate changes in charge-transfer resistance and phase response as a function of potassium-ion concentration, and the anodic current and phase deflection were subsequently extracted from the impedance data and correlated with the transistor's sensing performance, following the approach of Pecqueur et. al. [34].

3. Results and Discussion

3.1 Output Characteristics of Potassium-Selective OECT

Figure 3 presents the output characteristics of the potassium-selective OECT measured at KCl concentrations ranging from 0.0001 M to 1.67 M; the corresponding characteristics for the Tween 80-modified device are provided in Figure S3. The drain current increased with increasing drain voltage while exhibiting effective gate modulation across all potassium concentrations, confirming proper transistor operation.

At low potassium concentrations (0.0001–0.01 M), only modest modulation of the drain current was observed due to limited ionic transport through the ion-selective membrane. As the potassium concentration increased to 0.1 M and above, larger changes in drain current were obtained, indicating enhanced ionic conductivity and more efficient gating of the PEDOT:PSS channel.

At the highest KCl concentrations, 0.67 M and 1.67 M, the separation between output curves recorded at different gate voltages became markedly more pronounced, reflecting stronger transistor amplification. The increased ionic strength facilitates potassium ion transport through the membrane and promotes dedoping of the PEDOT:PSS channel, producing larger modulation of channel conductivity; this concentration dependence is examined more directly through the transfer characteristics below.

The improved modulation at higher KCl concentrations can be attributed to increased ionic conductivity and more efficient transport of K^+ ions through the ion-selective membrane [23], [24]. The transported ions induce electrochemical dedoping of the PEDOT:PSS channel, thereby changing its conductivity and modulating the drain current [35], [36]. These results confirm that

the printed OECT successfully transduces potassium ion concentration into an amplified electrical signal.

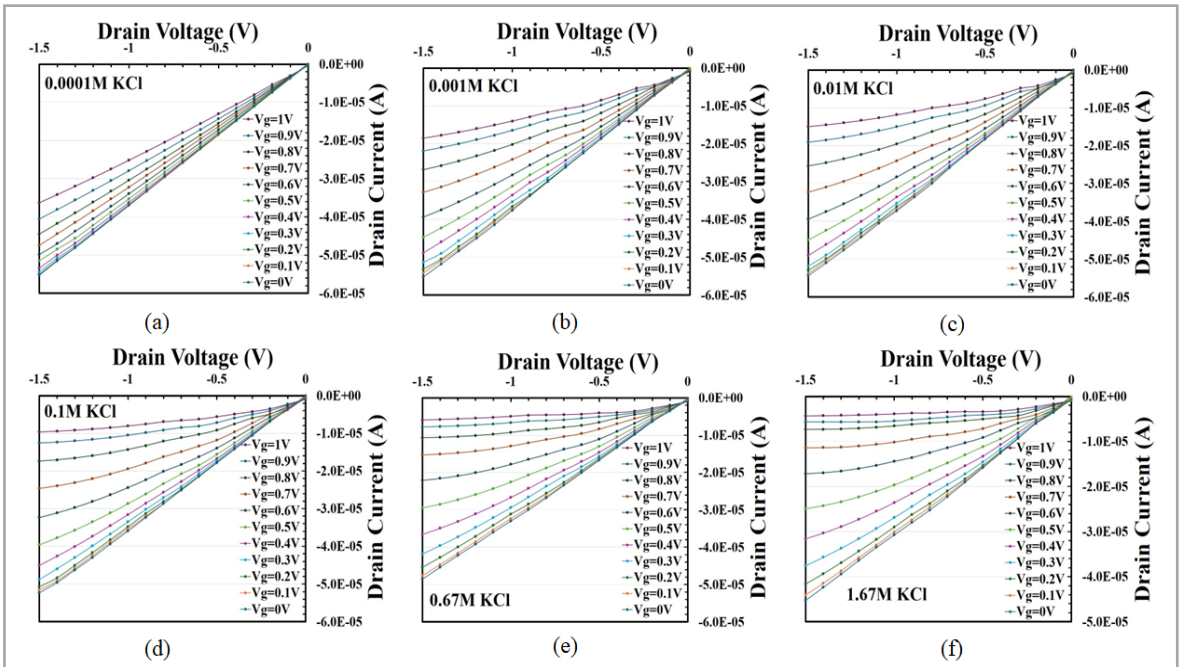


Figure 3. Output characteristics of the potassium-selective OECT measured in KCl solutions of varying concentrations from 0.0001 M to 1.67 M under different gate voltages.

3.2 Transfer Characteristics of Potassium-Selective OECT

Figure 4 presents the transfer characteristics of the potassium-selective OECT (PEG-modified PEDOT:PSS), measured over a KCl concentration range of 1.0×10^{-4} to 1.67 M; the corresponding characteristics for the Tween 80-modified device are provided in Figure S4. The device exhibited typical depletion-mode behavior, with the drain current decreasing progressively as the positive gate voltage increased. This behavior results from the injection of cations into the PEDOT:PSS channel, which compensates the positively charged PEDOT chains and causes electrochemical dedoping [37], [38], so that channel conductivity and drain current both decrease.

The transfer curves shifted systematically with increasing KCl concentration. At a given gate voltage, the drain current decreased as the potassium concentration increased, with the largest current suppression observed at 0.67 and 1.67 M. This concentration-dependent modulation is consistent with increased K^+ transport through the ion-selective membrane and stronger ionic gating of the OECT channel. At higher concentrations, the increased activity of K^+ produces stronger ionic gating and more extensive dedoping of PEDOT:PSS. The clear separation among the transfer curves demonstrates the ability of the OECT to convert variations in potassium concentration into measurable electrical responses. This behavior is same as the ion sensing from OECT [16], [19], [35].

The change in drain current, ΔI_D, also increased monotonically with potassium concentration, as shown in Figure 5a. The corresponding calibration relationship was

$$\Delta I_D = 2.0 \times 10^{-6} \log_{10}[K^+] + 3.0 \times 10^{-5} \quad (1)$$

with $R^2 = 0.9918$. Therefore, the current sensitivity was equivalent to

$$S_{\Delta I_D} = (2.0\ \mu\text{A})\ln(10) = 4.61\ \mu\text{A decade}^{-1} \quad (2)$$

The sensor therefore demonstrated a current sensitivity of approximately 4.61 μA decade⁻¹. The high linearity of both calibration plots confirms reliable potassium quantification over more than

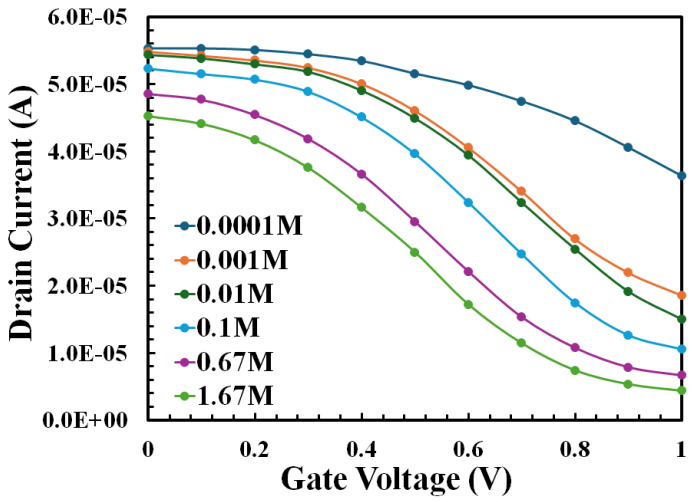


Figure 4. Transfer characteristics of the screen-printed potassium-selective organic electrochemical transistor (OECT) measured in KCl solutions with concentrations ranging from 0.0001 M to 1.67 M at drain voltages of -2V

four orders of magnitude in concentration. These devices show improvement compared with other reported K^+ ISM-based electrolyte gated-organic electrochemical transistor sensors [23], [24]. The lowest experimentally evaluated concentration was 1.0×10^{-4} M, corresponding to 0.1 mM KCl or approximately 3.91 ppm K^+.

The analyte-induced membrane potential (E_m), which depends logarithmically on the analyte activity (or approximately its concentration), can be described by the Nernst equation [39]:

$$E_m = E^0 + \frac{kT}{ne} \ln[M^{n+}] \quad (3)$$

where $E^0$is the standard potential, $k$is the Boltzmann constant, $T$is the absolute temperature, $n$is the ionic charge number, $e$is the elementary charge, and $[M^{n+}]$represents the activity or concentration of the target ion. The analyte-induced variation in $E_m$modulates the effective gate potential according to

$$V_{G,\text{eff}} = V_G + E_m \quad (4)$$

Consequently, the observed decrease in the drain–source current (I_{DS}) reflects a shift in $V_{G,\text{eff}}$. By correlating the I_{DS}change with the device transfer characteristics, the effective gate-potential shift—and hence the membrane potential E_m—can be quantitatively determined.

The equivalent gate-voltage shift, ΔV_G, was extracted from the transfer characteristics[40] and plotted against potassium concentration, as shown in Figure 5b. The calibration response followed

$$\Delta V_G = 0.0598 \log_{10}[K^+] + 0.6626 \quad (5)$$

with a coefficient of determination of $R^2 = 0.9953$. Expressed on the more commonly reported base-10 logarithmic scale, the sensitivity was calculated as

$$S_{\Delta V_G} = 0.0598 \ln(10) = 0.1377 \text{ V decade}^{-1} \quad (6)$$

Thus, the effective potential-shift sensitivity of the potassium-selective OECT was approximately 137.7 mV decade⁻¹.

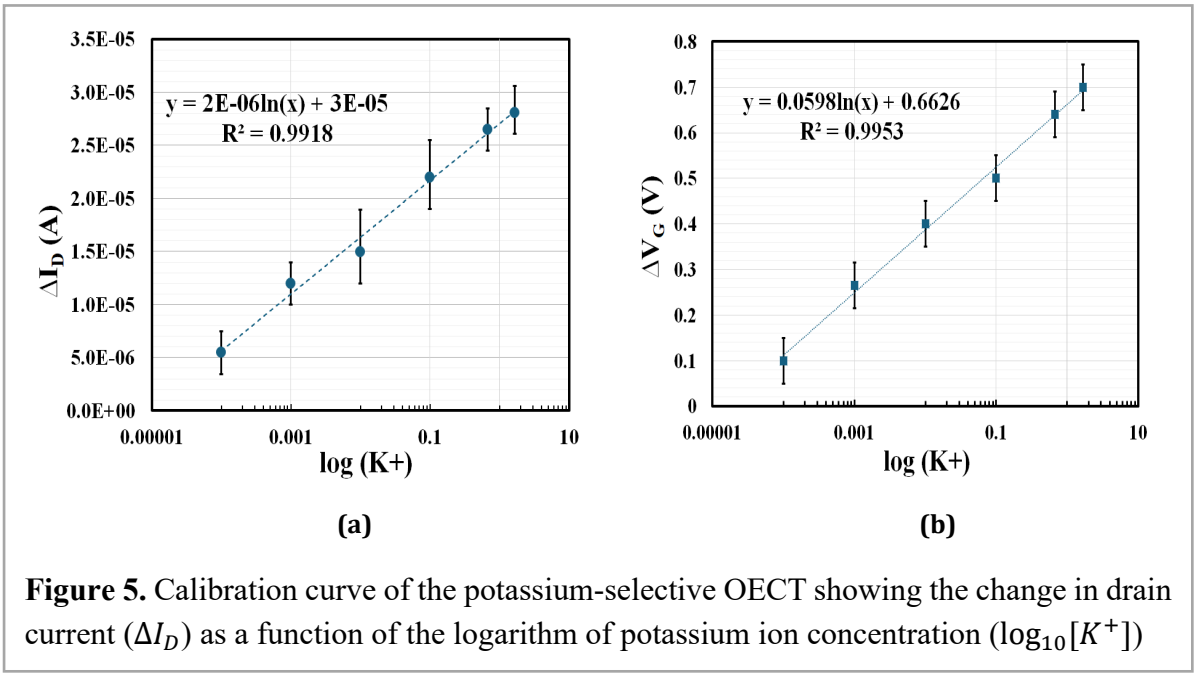


Figure 5. Calibration curve of the potassium-selective OECT showing the change in drain current (ΔI_D) as a function of the logarithm of potassium ion concentration ($\log_{10}[K^+]$)

3.3 Transient Response Analysis

The dynamic response of the potassium-selective OECT was evaluated by applying two consecutive gate-voltage pulses between 0 and 1 V. The applied gate-voltage waveform is shown in Figure 6. Each voltage level was maintained for approximately 10 s, giving a complete pulse period of 20 s. Figure 6 also presents the corresponding transient drain-current response measured at KCl concentrations ranging from 1.0×10^{-4} to 1.67 M.

When the gate voltage increased from 0 to 1 V, the drain current increased rapidly and then relaxed toward a quasi-steady-state value, reaching its initial maximum approximately 4–5 s after the beginning of each pulse before decreasing slightly to the plateau. This initial overshoot is attributed to rapid electrical double-layer charging and ion accumulation at the electrolyte/device interfaces, whereas the following relaxation reflects slower K^+ transport through the ion-selective membrane and redistribution within the volumetric PEDOT:PSS channel.

When the gate voltage returned from 1 to 0 V, an opposite current transient was observed. The current initially crossed the baseline and reached a negative minimum before gradually returning toward zero. This reverse transient is associated with the discharge of the electrochemical interfaces and the redistribution or extraction of ions accumulated during the positive gate pulse[13]. The opposite responses during application and removal of the gate voltage demonstrate reversible electrochemical modulation of the OECT channel [41].

The magnitude of the transient drain-current response increased systematically with KCl concentration. At 1.0×10^{-4}, 1.0×10^{-3}, and 0.01 M, relatively small current changes were recorded because of the lower ionic conductivity and limited K^+ flux through the ion-selective membrane. A substantially larger response was obtained at 0.1 M, reaching approximately 40 µA during the positive gate pulse.

At 0.67 M KCl, the positive current reached approximately 84 µA before stabilizing near 79 µA, while the reverse transient reached approximately −36 µA. The largest response was observed at 1.67 M KCl, where the positive current reached approximately 134 µA and stabilized near 123 µA, and returning the gate voltage to 0 V produced a negative transient of approximately −105 µA. This increase in transient-current magnitude at higher concentrations is consistent with greater K^+ availability, increased electrolyte conductivity, reduced ionic resistance, and more efficient ion transport through the selective membrane.

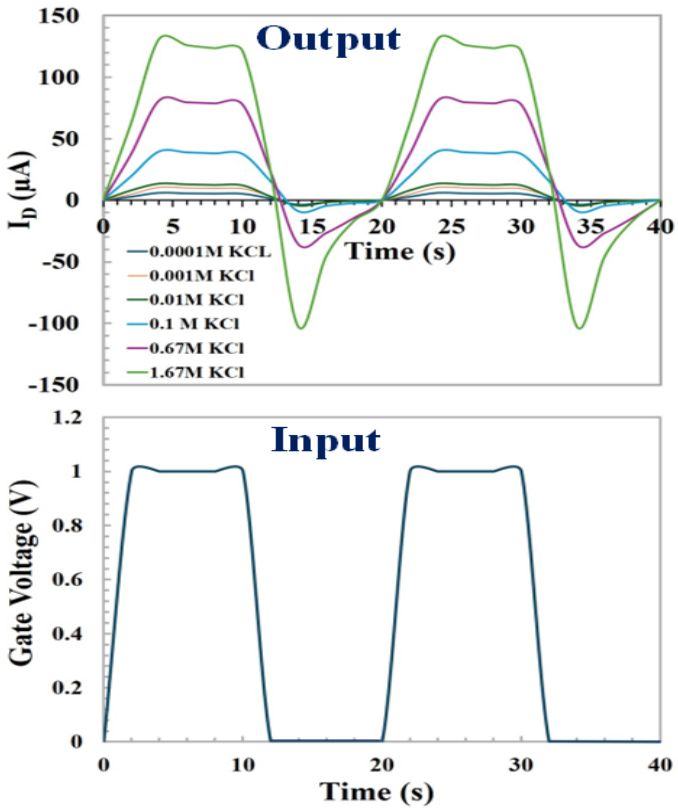


Figure 6. Transient characterization of the potassium-selective OECT, **Input:** applied gate-voltage waveform alternating between 0 and 1 V at approximately 10 s intervals and **Output:** corresponding transient drain-current responses measured at KCl concentrations ranging from $1.0 \times 10^{-4}$to 1.67 M. The increasing current modulation with KCl concentration and the similar responses during consecutive cycles demonstrate concentration-dependent sensing, reversible ionic modulation, and short-term operational stability.

Nearly identical transient profiles were obtained during the two successive pulse cycles. The peak currents, plateau currents, reverse-current minima, and recovery behavior all remained consistent between the first and second cycles, similar to the transient behavior reported for OECTs under other target ions[19], [41], [42]. No substantial baseline drift was observed over the 40 s measurement period, demonstrating reversible ionic modulation, repeatable switching, and short-term operational stability. The rise and fall times also decreased with increasing K^+concentration, indicating faster switching at higher concentrations. The rise and fall times, defined respectively as the time for the current to change from 10% to 90% of its steady-state value after the rising edge and from 90% to 10% after the falling edge, both decreased with increasing K^+ concentration, indicating faster switching at higher concentrations. At low KCl concentrations, the smaller number of available charge carriers and higher ionic resistance slow the formation and relaxation of the interfacial double layers, and transport through the ion-selective membrane may also become rate-limiting, resulting in longer rise and fall times. As the KCl concentration increases, the solution resistance decreases and the ionic current increases; because the characteristic charging time can be approximated by [13]:

$$\tau = R_{\text{ion}} C_{\text{eff}} \tag{7}$$

where R_{ion} is the effective ionic resistance and C_{eff} is the combined interfacial and volumetric capacitance, a reduction in R_{ion} produces a smaller time constant and therefore a faster response[43]. The larger K^+ concentration gradient also increases the driving force for ion transport through the membrane, allowing the membrane potential and channel charge state to reach equilibrium more rapidly, while on the falling edge improved ionic conductivity similarly promotes faster double-layer discharge and more rapid redistribution of ions, reducing the recovery time [44]. The observed concentration dependence of the rise and fall times is therefore consistent with an ion-transport- and resistance-limited switching mechanism [13], [16], [45].

Overall, the transient measurements demonstrate a rapid, reversible, and concentration-dependent electrical response. The increased transient-current amplitude at higher KCl concentrations agrees with the transfer-characteristic results above and is examined further below through cyclic voltammetry and impedance spectroscopy, which provide complementary electrochemical evidence for the same coupling between K^+ transport and electronic conduction in the PEDOT:PSS channel.

3.4 Cyclic Voltammetry Analysis

Cyclic voltammetry was performed to further investigate the electrochemical processes responsible for the concentration-dependent response of the potassium-selective OECT. Figure 7 presents the cyclic voltammograms recorded over a potential range of approximately −1.0 to +1.0 V in KCl solutions ranging from 1×10^{-4} to 1.67 M. The magnitudes of both the anodic and cathodic currents increased systematically with increasing KCl concentration, indicating enhanced ionic transport and electrochemical charging of the device.

At the lowest concentrations of 1.0×10^{-4} and 1.0×10^{-3} M, relatively small currents were observed throughout the potential sweep. This behavior is attributed to the relatively low ionic conductivity of the electrolyte and the limited availability of mobile ions for interfacial and volumetric charge compensation. As the concentration increased to 0.01 and 0.1 M, the voltammograms became progressively broader and the current increased, indicating enhanced ion transport, electrical double-layer charging, and electrochemical interaction with the PEDOT:PSS

channel [18]. Ion diffusion into the bulk of mixed ionic-electronic conducting polymers is a major contributor to their voltammetric response, while capacitive and pseudocapacitive processes can also contribute to the measured current [46], [47].

A substantially larger electrochemical response was observed at 0.67 and 1.67 M KCl. At 1.67 M, the anodic and cathodic currents reached approximately +58 and −58 µA, respectively, whereas peak-current magnitudes of approximately 41 µA were obtained at 0.67 M. Increasing the electrolyte concentration provides a larger reservoir of mobile ions and increases ionic conductivity, thereby facilitating ion transport through the potassium-selective membrane and ion exchange with the PEDOT:PSS channel. Consequently, a greater amount of electrochemical charge can be transferred or stored during each potential sweep, producing larger anodic and

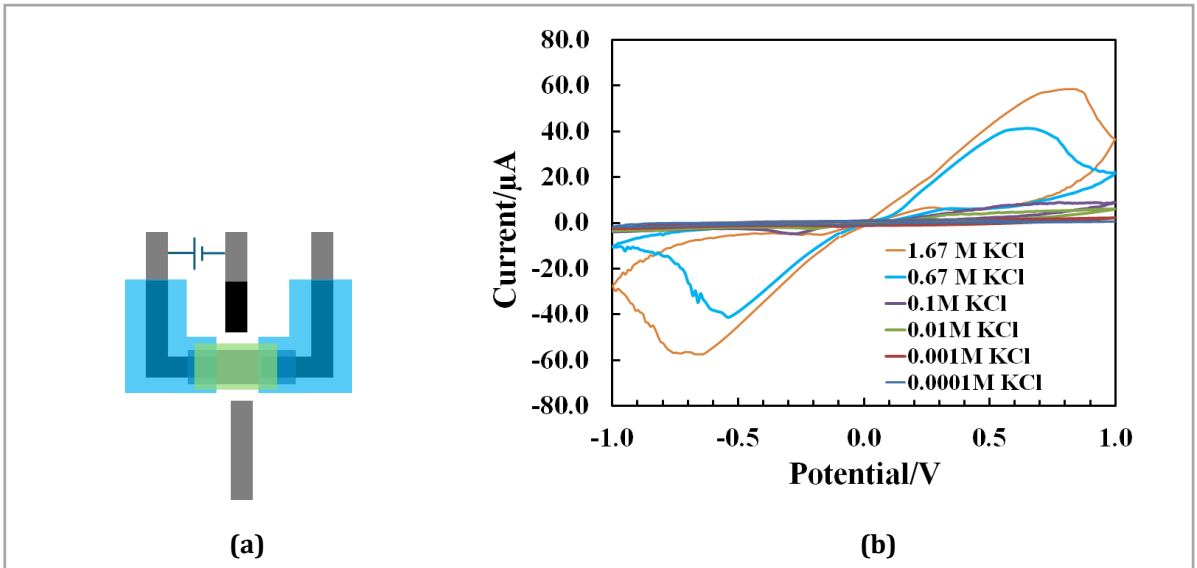


Figure 7. Cyclic voltammograms of the potassium-selective OECT measured in KCl solutions with concentrations ranging from $1.0 \times 10^{-4}$to 1.67 M. The increasing anodic and cathodic current magnitudes with KCl concentration indicate enhanced ionic conductivity, K^+ transport, and electrochemical modulation of the PEDOT:PSS channel.

cathodic currents. The broad voltammetric features, rather than sharply defined redox peaks, suggest that the measured response contains overlapping contributions from electrical-double-layer charging, volumetric or pseudocapacitive charging of PEDOT:PSS, and reversible Faradaic oxidation–reduction processes. Similar CV responses in OECT materials have been used to evaluate polymer capacitance, ion uptake, oxidation potential, and native doping state [47], [48].

The broad anodic and cathodic features, rather than sharply defined redox peaks, suggest that the measured response contains contributions from both non-Faradaic capacitive charging and Faradaic electrochemical processes [49]. During the positive-going potential sweep, oxidation of the PEDOT:PSS channel and associated ionic redistribution produce an increasing anodic current, while during the reverse sweep, reduction and dedoping of PEDOT:PSS, accompanied by K^+ incorporation or redistribution, generate the cathodic response. The hysteresis between the forward and reverse scans reflects the finite time required for ion transport through the ion-selective membrane and within the volumetric PEDOT:PSS channel[19], [24], [35], [50].

Importantly, the increase in voltammetric current with KCl concentration does not contradict the decrease in drain current observed in the output characteristics. The two measurements represent different physical quantities. The drain current, measures the steady-state electronic conduction between the source and drain electrodes and is therefore governed primarily by the hole density and mobility in the PEDOT:PSS channel. At a given positive gate bias, increasing the KCl concentration enhances the transport of K^+ through the ion-selective interface and promotes greater incorporation of cations into the PEDOT:PSS phase. These cations compensate the negatively charged PSS groups and reduce oxidized $PEDOT^+$ charge carriers according to the simplified reaction:

$$PEDOT^+:PSS^- + K^+ + e^- \leftrightarrow PEDOT^o + K^+:PSS^- \quad (8)$$

The resulting reduction, or dedoping, of PEDOT decreases the hole concentration and therefore decreases the magnitude of the source–drain current.

In contrast, the current measured during CV represents the rate of electrochemical charge exchange during a continuously varying potential, approximately $i_{CV} = dQ/dt$. A higher KCl concentration enables more rapid ion transport and a larger amount of charge compensation, double-layer charging, and reversible volumetric doping/dedoping during the potential sweep. Therefore, stronger dedoping can simultaneously produce a lower electronic drain current and a larger electrochemical current. In other words, the decreasing drain current and increasing CV-current magnitude are complementary manifestations of the same concentration-enhanced ionic coupling: the former reflects the resulting loss of electronic charge carriers in PEDOT:PSS, whereas the latter reflects the greater rate and amount of ion-coupled electrochemical charge exchanged during the potential sweep. The channel conductivity also need not vary linearly with electrochemical or electrolyte potential because it depends on the voltage-dependent doping state and charge-carrier mobility of the polymer [47].

During the reverse potential sweep, the direction of ion redistribution and electron transfer is reversed, producing the corresponding cathodic response and partially restoring the oxidized, electronically conducting state of PEDOT:PSS. The hysteresis between the forward and reverse scans reflects the finite time required for K^+ transport through the ion-selective membrane and for ionic redistribution within the volumetric PEDOT:PSS channel. Overall, the concentration-dependent increase in anodic and cathodic currents confirms increasingly strong electrochemical coupling between the potassium-selective interface and the PEDOT:PSS channel and provides complementary evidence for the ion-induced drain-current modulation observed in the transistor measurements.

3.5 Electrochemical Impedance Spectroscopy Analysis

Electrochemical impedance spectroscopy was performed to evaluate the interfacial charge-transfer and ion-transport behavior of the potassium-selective OECT at KCl concentrations ranging from 1.0×10^{-4} to 1.67 M. Figure 8a presents the corresponding Nyquist plots, and Figure 8b shows the frequency-dependent phase response over the range of 10 Hz to 10 kHz.

The Nyquist plots exhibit concentration-dependent semicircular features followed by low-frequency tails, indicating that the device response contains contributions from solution resistance, interfacial charge-transfer resistance, nonideal double-layer capacitance, and ion diffusion through the potassium-selective membrane. The semicircular response can be represented approximately by an equivalent circuit comprising the solution resistance, R_s, in series with a parallel combination

of charge-transfer resistance, R_{ct}, and a constant-phase element [33], [43]. A diffusion-related element may also be included to describe ion transport through the membrane and electrolyte[34].

At 1.0×10^{-4} M KCl, the Nyquist plot exhibited the largest overall impedance and the widest semicircular feature, indicating a relatively high interfacial and membrane resistance that results from the low ionic conductivity of the solution and the limited availability of mobile K^+ ions. As the KCl concentration increased, the impedance response shifted toward lower values of Z' and Z'', and the substantial reduction in semicircle size observed at 0.67 and 1.67 M indicates a

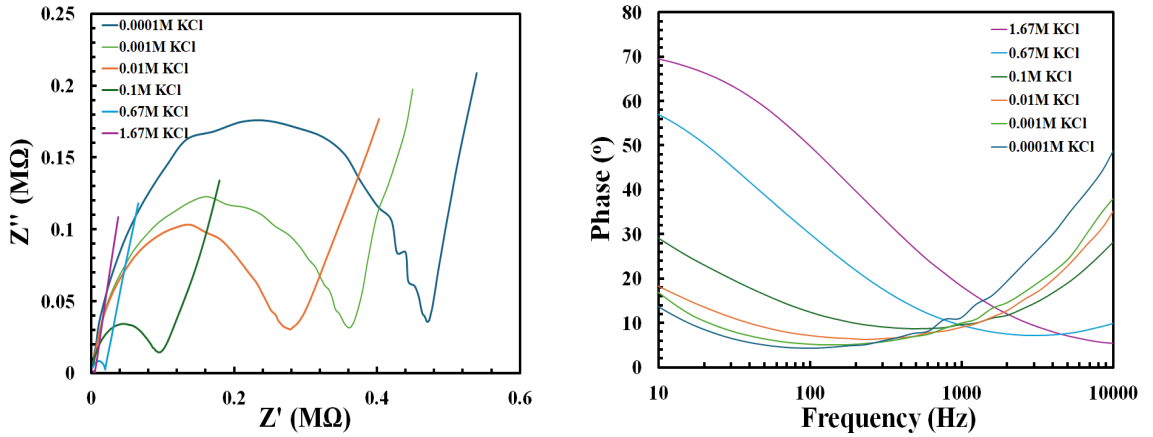


Figure 8. Electrochemical impedance response of the potassium-selective OECT measured in KCl solutions ranging from $1.0 \times 10^{-4}$to 1.67 M: (a) Nyquist plots showing a concentration-dependent decrease in electrochemical impedance and (b) phase-angle spectra illustrating changes in interfacial polarization and capacitive behavior as a function of frequency and KCl concentration.

decrease in the effective charge-transfer and ion-transport resistances.

This concentration-dependent reduction in impedance can be attributed to the increased ionic conductivity of the electrolyte and the greater number of K^+ ions available for transport through the ion-selective membrane[20], [50]. At higher concentrations, more efficient ionic transport facilitates charge compensation at the electrolyte/electrode and electrolyte/PEDOT:PSS interfaces. Consequently, the electrochemical modulation of the PEDOT:PSS channel occurs more readily. The Nyquist plots result therefore support the progressively larger drain-current modulation and voltammetric currents observed at increasing potassium concentrations.

The phase-angle spectra provide further information about the change in the electrochemical response with potassium concentration. At low frequencies, the phase angle increased substantially with concentration, reaching approximately 56°for 0.67 M and 69°for 1.67 M KCl at 10 Hz. These larger phase angles indicate an increasingly capacitive response arising from enhanced electrical double-layer formation, ion accumulation, and volumetric charging of the PEDOT:PSS channel[51], whereas the lower-concentration solutions exhibited smaller low-frequency phase angles, consistent with responses dominated more strongly by resistive limitations associated with the electrolyte and ion-selective membrane.

For the 1.67 M solution, the phase angle decreased continuously with increasing frequency, approaching approximately 5° at 10 kHz, indicating that ion accumulation and interfacial polarization dominate at low frequencies while the system becomes increasingly resistive at higher frequencies as ions can no longer fully follow the rapidly varying electric field[52]. The 0.67 M solution exhibited a similar trend, although its phase angle reached a minimum at a higher value. The dilute solutions displayed more complex high-frequency behavior, which may originate from overlapping interfacial relaxation processes, membrane capacitance, contact effects, and parasitic contributions from the measurement configuration[53].

Overall, the EIS results demonstrate that increasing potassium concentration reduces the effective electrochemical impedance and enhances the capacitive and ion-transport response of the OECT. These observations are consistent with the cyclic-voltammetry and transfer-characteristic measurements and confirm that the potassium-selective membrane effectively couples concentration-dependent K^+ transport to the electronic conductivity of the PEDOT:PSS channel. Because selective ion transport is central to this sensing mechanism, the following section examines whether the device response is specific to K^+ relative to other physiologically and environmentally relevant cations.

3.6 Selectivity Analysis

The selectivity of the potassium-sensitive OECT was investigated using three complementary characterization methods: transistor output characteristics, cyclic voltammetry (CV), and electrochemical impedance spectroscopy (EIS). KCl was compared with potentially interfering electrolytes containing NH_4^+, Na^+, Mg^{2+}, and Ca^{2+}, with measurements performed both in individual electrolyte solutions and after adding the interfering salts to 0.1 M KCl.

3.6.1 Comparison Based on I–V Characteristics

The output characteristics of the OECT were measured in KCl, NH_4Cl, NaCl, $MgCl_2$, and $CaCl_2$ by sweeping the drain voltage from 0 to −1.5 V while varying the gate voltage from 0 to 1.0 V (Figure 9). The device exhibited p-type depletion-mode operation in all electrolytes, with the magnitude of the drain current decreasing as the positive gate voltage increased; however, the extent of gate-induced current modulation depended strongly on the cation present in the electrolyte.

At $V_D = -1.5$ V, the drain-current modulation, ΔI_D, was approximately 19 μA in KCl. By comparison, ΔI_Dvalues of approximately 14.5, 11.5, 8, and 4 μA were measured in NH_4Cl, NaCl, $MgCl_2$, and $CaCl_2$, respectively. Therefore, the K^+ response was approximately 1.3, 1.7, 2.4, and 4.8 times greater that of responses to NH_4^+, Na^+, Mg^{2+}, and Ca^{2+}, respectively.

The enhanced response to K^+ is attributed to the preferential complexation of potassium ions by ionophere III within the ion-selective membrane, whose cavity size and coordination geometry are particularly favorable for K^+ transport. This selective interaction changes the interfacial potential at the functionalized gate and produces stronger electrochemical gating of the PEDOT:PSS channel. Consequently, greater channel dedoping and drain-current modulation are observed in KCl. In contrast, the smaller Na^+ ion and the divalent Ca^{2+} and Mg^{2+} ions interact less favorably with the ionophere III -based membrane, resulting in weaker OECT responses. Among the interfering ions, NH_4^+ produced the highest response which can be associated with the similarity between the effective size and coordination behavior of NH_4^+ and K^+; nevertheless, the KCl response remained clearly higher than the NH_4Cl response. These results demonstrate that the

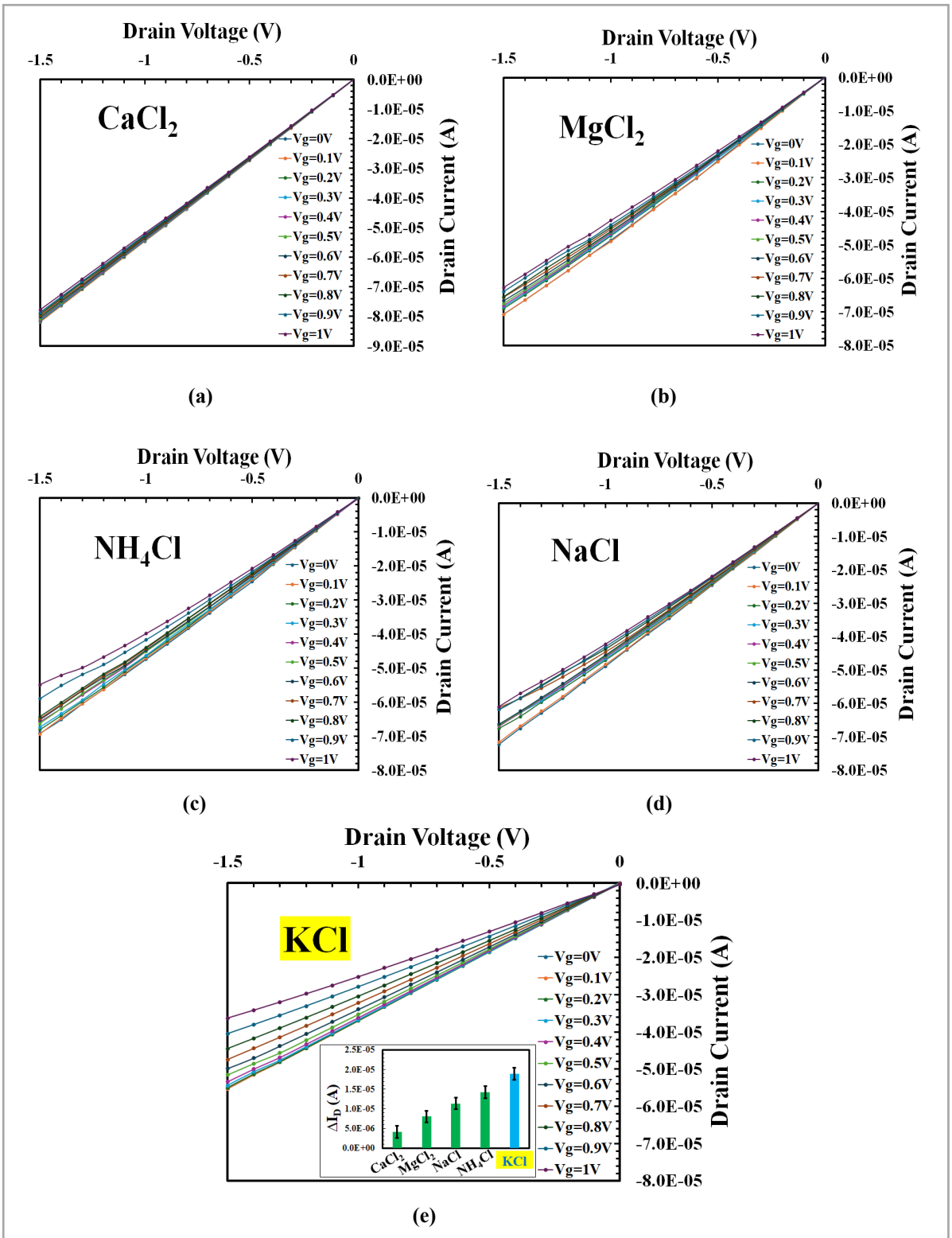


Figure 9. Output characteristics of the potassium-selective OECT measured in the presence of (a) $CaCl_2$, (b) $MgCl_2$, (c) NaCl, (d) NH_4Cl, and (e) KCl, with V_G varied from 0 to 1.0 V. The inset compares the drain-current modulation, ΔI_D, measured at $V_D = -1.5$V, demonstrating the strongest response toward K^+. Error bars represent the standard deviation from replicate measurements.

functionalized OECT exhibits preferential sensitivity toward K^+ over the tested physiologically

and environmentally relevant interfering ions.

3.6.2 Comparison Based on Cyclic Voltammetry

CV measurements provide complementary, independent evidence for this electrical selectivity. Figure 10(a) compares the CV responses obtained separately in KCl, NH_4Cl, NaCl, $MgCl_2$, and $CaCl_2$. The KCl solution produced a substantially greater electrochemical current and more pronounced redox features than the other electrolytes: the anodic response in KCl reached approximately 11 μA near 0.32 V, whereas the interfering electrolytes produced much smaller and broader responses, generally below approximately 3 μA. A considerably larger cathodic current was also observed for KCl during the reverse scan, indicating more effective ion-membrane interaction and interfacial charge transfer in the presence of K^+.

The interference experiment in Figure 10 (b) further compares 0.1 M KCl with KCl solutions containing NH_4Cl, NaCl, $MgCl_2$, or $CaCl_2$. Pure 0.1 M KCl generated the largest anodic and cathodic peak currents, reaching approximately $+33$ and -32 μA, respectively; the addition of the interfering salts decreased the peak-current magnitude to different extents, giving the approximate anodic peak-current order was

$$KCl > KCl + NaCl > KCl + NH_4Cl > KCl + MgCl_2 > KCl + CaCl_2.$$

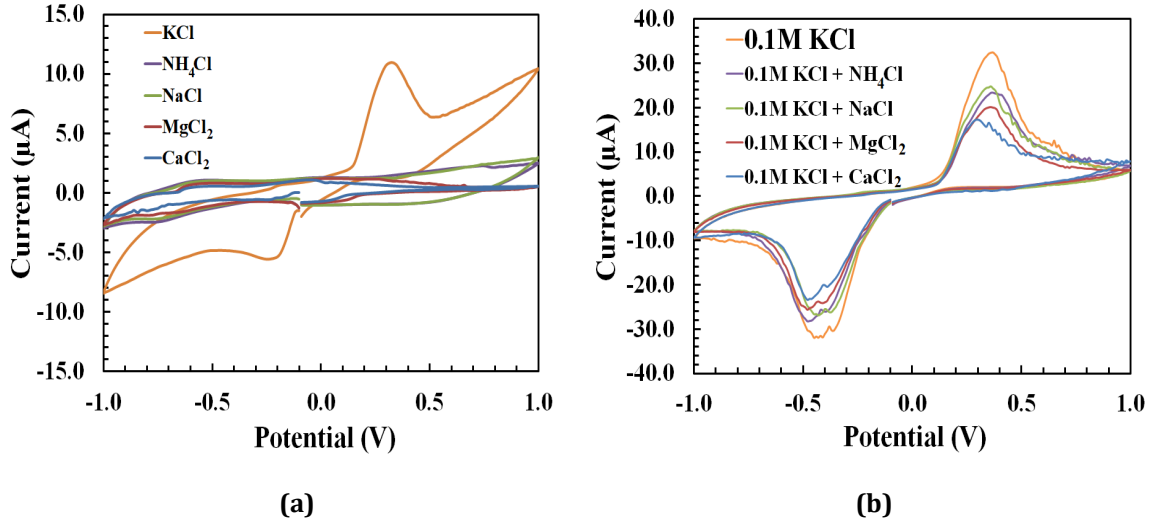


Figure 10. Selectivity characterization of the potassium-sensitive OECT: (a) cyclic voltammograms measured separately in KCl, NH_4Cl, NaCl, $MgCl_2$, and $CaCl_2$; (b) cyclic voltammograms of 0.1 M KCl before and after the addition of interfering electrolytes

Importantly, the principal oxidation and reduction features remained visible after the interfering ions were introduced. This indicates that the potassium-recognition process remained active in mixed-electrolyte environments, although the interfering ions partially suppressed the electrochemical response. This suppression may result from competitive ion accumulation, changes in ionic strength and activity, and modification of the interfacial double-layer structure[54]. The CV results therefore support the preferential electrochemical response of the ionophere III-functionalized electrode toward K^+.

3.6.3 Comparison Based on Electrochemical Impedance Spectroscopy

The EIS phase spectra provide additional information about frequency-dependent ion transport and interfacial polarization. For the individual electrolyte solutions in Figure 11(a), the largest low-frequency phase angle was observed in KCl. At approximately 5 Hz, the phase angle was about 31°for KCl, compared with approximately 25°, 21°, 19°, and 17°for NH_4Cl, NaCl, $MgCl_2$, and $CaCl_2$, respectively. The selectivity was most evident in the low-frequency region, where ion partitioning, interfacial polarization, and membrane-related processes dominate the impedance response. At frequencies above approximately 100 Hz, the phase spectra gradually converged, indicating a reduced contribution from selective ion–membrane interactions.

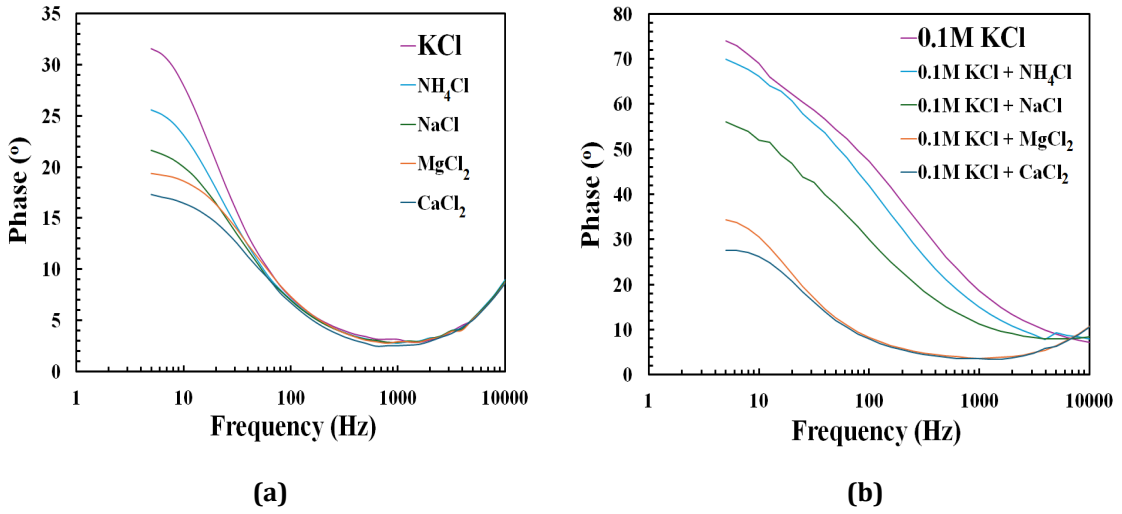


Figure 11. Selectivity characterization of the potassium-sensitive OECT: (a) EIS phase spectra measured separately in the different electrolytes; and (b) EIS phase spectra of 0.1 M KCl in the presence of interfering electrolytes.

A similar trend was observed when the interfering salts were added to 0.1 M KCl, as shown in Figure11 (b). Pure KCl displayed the highest low-frequency phase angle, approximately 74°at 5 Hz. After the addition of NH_4Cl, NaCl, $MgCl_2$, and $CaCl_2$, the corresponding phase angles decreased to approximately 69°, 56°, 34°, and 28°, respectively, giving the phase-angle order

$$KCl > KCl + NH_4Cl > KCl + NaCl > KCl + MgCl_2 > KCl + CaCl_2.$$

The higher phase angle in KCl indicates a stronger capacitive or polarization contribution associated with selective K^+ accumulation and complexation within the ionophere III-containing membrane[55]. Although the interfering ions altered the interfacial impedance, the KCl-containing solutions retained distinguishable low-frequency behavior. The convergence of the curves at higher frequencies suggests that the selectivity is primarily governed by relatively slow ion-transfer and membrane-polarization processes rather than by the high-frequency response of the electrolyte[56].

Overall, the I–V, CV, and EIS measurements consistently demonstrate preferential detection of K^+ over NH_4^+, Na^+, Mg^{2+}, and Ca^{2+}. The results also show that NH_4^+ is the most significant potential interferent based on the transistor and low-frequency EIS responses, whereas the divalent ions generally produce weaker responses.

3.7 Comparison with Previously Reported Potassium Sensors

Table 1 compares the analytical and fabrication characteristics of the proposed screen-printed OECT with previously reported potassium sensors based on potentiometric, coulometric, and transistor-based transduction. Conventional potentiometric sensors generally exhibit near-Nernstian voltage sensitivities of approximately 40–71 mV decade^{-1}, whereas OECT-based devices convert ion-induced interfacial-potential changes into amplified drain-current responses. Because the reported devices use different transduction mechanisms, output quantities, concentration ranges, electrolytes, device geometries, and operating conditions, their numerical sensitivity values should not be compared directly without considering the corresponding measurement conditions. The present device exhibited a current sensitivity of 4.61 μA decade^{-1} and an equivalent gate-voltage sensitivity of 137.7 mV decade^{-1}, with linear calibration coefficients of R^2 = 0.9918 and 0.9953, respectively. Although several previously reported OECTs provide larger current sensitivities or lower detection limits, the proposed platform offers an exceptionally broad experimentally evaluated concentration range of 1.0×10^{-4}–1.67 M, and it combines scalable multilayer screen printing with transistor calibration, transient switching, cyclic voltammetry, electrochemical impedance spectroscopy, and interference analysis on the same potassium-selective device. This combination provides both an amplified electrical response and complementary information about ion transport, interfacial charge transfer, and selectivity, supporting the platform's potential for potassium monitoring across agricultural, environmental, and point-of-care applications.

Table 1. Comparison of the sensing mechanism, materials, sensitivity, limit of detection, and detection range of the proposed screen-printed potassium-selective OECT with previously reported potassium-ion sensors

Sensor Type	Transduction Mechanism	Sensing material	Sensitivity	LOD	Detection Range	Reference
Potentiometric	All-solid-state K^+ ISE ion exchange	Graphite–epoxy solid contact/PVC–DOS–valinomycin–KTCPB membrane; Cu reference	69.4–71.2 mV/dec	10^{-4} M	10^{-4} -10^{-1}M	[6]
Potentiometric	$KSr_2Nb_5O_{15}$ with extraction/insertion topotactic processes of the potassium ions	Carbon paste electrode modified (CPEM) with a novel $KSr_2Nb_2O_{15}$.	51.1 mV/dec	7.27 x 10^{-5} mol/L	1.26 x 10^{-5} at 1.62 x 10^{-3} mol/L	[57]
Potentiometric	PEDOT or POT as a	PET/ Pt/C/PEDOT or	54.3 ± 1.5 mV/dec for POT;	10^{-4} M	10^{-4} -10^{-1}M	[58]

	conductive polymer	POT/EDOT (97%) in EMIM NTf2 (99.5%)	45.7± 7.4 mV/dec for PEDOT			
Floating gate OECT	Solid-state ionic conductor (SSIC)	Au Source-Draain/PEDOT:PSS/ PSS:Na/ EMIM-TFSI	40 mV/dec	0.011 mM	10^{-6} -10^{-1} M	[21]
Multichannel OECT	Multi ion detection- Na+, K+, Ca+	PEN/Ti-Au/PEDOT: PSS/ISM/K+ ISM	59.2 mV/dec; 1.04 mA/dec	0.0049 2 mM	3.4–21 mM	[24]
Coulometric solid-contact K^+ sensor	Constant-potential coulometry	nPt-LIG/TTF/PVC-DOS/valinomycin	168.2 µC/dec	0.10 mM	11–22 mM	[9]
Wearable potentiometric	Open-circuit potential (OCP)	Carbon/PEDOT:PSS/valinomycin-NaTPB-PVC-DOS	161 mV/dec	NR	2–32 mM	[59]
EWOD-integrated K^+ ion-selective sensor	Potentiometric EMF	Cr/Au/Ag/AgCl/ potassium ionophore ISM	58 mV/dec	10^{-6} M	10^{-6} -10^{-1} M	[8]
Implantable wire-based K^+ ISE	Potentiometric OCP	Cu/Pd/PEDOT:PSS/K^+-selective membrane	52.778 ± 2.51 mV/dec	$10^{-5.16}$ M	10 µM–100 mM	[60]
OECT	K^+ insertion/extraction-mediated PB redox response	Ag/Ag-AgCl/PEDOT:PSS/Dielectric/NaCl/K+ Ionophere III ISM	170 µA/dec; 99 mV/dec	10^{-5} M	2-30 mM	[23]
Ion-selective OECT	Valinomycin as K+ ionophore.	Au/ PEDOT:PSS/ K_2HPO_3	2.50 mA/dec	NR	0.1 mM to 100 mM	[10]
Paper based OECT	K^+-induced PEDOT doping/dedoping and drain-	Paper/ Au/ PEDOT:PSS/ K+ ISM	67.3 mV/dec	NR	2.4-5.75 mM	[22]

	current modulation					
Textile based OECT	K^+-induced PEDOT:PSS doping	Acrylic textile thread/Potassium selective membrane	3.49 M^{-1}	10^{-5} M	10^{-5} to 1 M	[18]
Screen-printed OECT—this work	K^+-induced PEDOT:PSS doping/dedoping and drain-current modulation	Ag/C/PEDOT:PSS/ K^+-selective membrane	4.61 µA/dec; 137.7 mV/dec	0.1 mM	10^{-4} to 1.67 M	This work

4. Conclusion

A multilayer screen-printed potassium-selective organic electrochemical transistor (OECT) was developed and systematically investigated using complementary electrical and electrochemical characterization techniques. The device exhibited concentration-dependent modulation of the drain current over a KCl concentration range of 1.0×10^{-4} to 1.67 M, with a current sensitivity of 4.61 µA decade^{-1} (R^2 = 0.9918) and an equivalent gate-voltage-shift sensitivity of 137.7 mV decade^{-1} (R^2 = 0.9953). Transient measurements demonstrated reversible and concentration-dependent switching, with increased current modulation and faster response at higher K^+ concentrations. Cyclic voltammetry showed increasing anodic and cathodic current magnitudes with increasing KCl concentration, while electrochemical impedance spectroscopy revealed concentration-dependent changes in impedance and low-frequency capacitive behavior. Selectivity measurements further demonstrated a preferential response to K^+ over NH_4^+, Na^+, Mg^{2+}, and Ca^{2+}. Together, the electrical, transient, voltammetric, and impedance measurements demonstrate the coupling between selective K^+ transport, interfacial electrochemical processes, and modulation of electronic conduction in the PEDOT:PSS channel. The results establish the multilayer screen-printed OECT as a scalable platform for investigating ion-selective transduction and potassium sensing. Future studies will focus on long-term stability, device-to-device reproducibility, and validation in complex sample matrices.

Acknowledgements

The authors acknowledge institutional support from Northern Illinois University, ASM and AR are supported by startup funds by the University of Texas Rio Grande Valley and the research fellow year 2 seed award by the college of health professions , UTRGV, and thank all collaborators who contributed insights during the preparation of this paper.

References

[1] B. F. Palmer and D. J. Clegg, "Physiology and Pathophysiology of Potassium Homeostasis: Core Curriculum 2019," *American Journal of Kidney Diseases*, vol. 74, no. 5, pp. 682–695, Nov. 2019, doi: 10.1053/j.ajkd.2019.03.427.

[2] F. Arshadi *et al.*, “A miniaturized electrochemical biosensor for real-time in vivo potassium monitoring in the inner ear,” *Biosens. Bioelectron.*, vol. 298, p. 118388, Apr. 2026, doi: 10.1016/j.bios.2026.118388.

[3] L. Ma, W. Hou, Z. Ji, Z. Sun, M. Li, and B. Lian, “Wearable Electrochemical Sensor for Sweat-Based Potassium Ion and Glucose Detection in Exercise Health Monitoring,” *ChemistryOpen*, vol. 13, no. 8, Aug. 2024, doi: 10.1002/open.202300217.

[4] P. Pirovano *et al.*, “A wearable sensor for the detection of sodium and potassium in human sweat during exercise,” *Talanta*, vol. 219, p. 121145, Nov. 2020, doi: 10.1016/j.talanta.2020.121145.

[5] J. Sardans and J. Peñuelas, “Potassium Control of Plant Functions: Ecological and Agricultural Implications,” *Plants*, vol. 10, no. 2, p. 419, Feb. 2021, doi: 10.3390/plants10020419.

[6] S. G. Lemos, A. R. A. Nogueira, A. Torre-Neto, A. Parra, J. Artigas, and J. Alonso, “In-Soil Potassium Sensor System,” *J. Agric. Food Chem.*, vol. 52, no. 19, pp. 5810–5815, Sep. 2004, doi: 10.1021/jf0492924.

[7] L. van de Velde, E. d’Angremont, and W. Olthuis, “Solid contact potassium selective electrodes for biomedical applications – a review,” *Talanta*, vol. 160, pp. 56–65, Nov. 2016, doi: 10.1016/j.talanta.2016.06.050.

[8] A. Farzbod and H. Moon, “Integration of reconfigurable potentiometric electrochemical sensors into a digital microfluidic platform,” *Biosens. Bioelectron.*, vol. 106, pp. 37–42, May 2018, doi: 10.1016/j.bios.2018.01.048.

[9] R. G. Hjort *et al.*, “Laser-Induced Graphene Decorated with Platinum Nanoparticles for Electrochemical Analysis of Saliva,” *ACS Appl. Nano Mater.*, vol. 6, no. 22, pp. 20801–20811, Nov. 2023, doi: 10.1021/acsanm.3c03786.

[10] M. Clua Estivill, A. Ait Yazza, P. Blondeau, and F. J. Andrade, “Ion-selective organic electrochemical transistors for the determination of potassium in clinical samples,” *Sens. Actuators B Chem.*, vol. 401, p. 135027, Feb. 2024, doi: 10.1016/j.snb.2023.135027.

[11] J. Rivnay, S. Inal, A. Salleo, R. M. Owens, M. Berggren, and G. G. Malliaras, “Organic electrochemical transistors,” *Nat. Rev. Mater.*, vol. 3, no. 2, p. 17086, Jan. 2018, doi: 10.1038/natrevmats.2017.86.

[12] H. S. White, G. P. Kittlesen, and M. S. Wrighton, “Chemical derivatization of an array of three gold microelectrodes with polypyrrole: fabrication of a molecule-based transistor,” *J. Am. Chem. Soc.*, vol. 106, no. 18, pp. 5375–5377, Sep. 1984, doi: 10.1021/ja00330a070.

[13] D. A. Bernards and G. G. Malliaras, “Steady-State and Transient Behavior of Organic Electrochemical Transistors,” *Adv. Funct. Mater.*, vol. 17, no. 17, pp. 3538–3544, Nov. 2007, doi: 10.1002/adfm.200601239.

[14] H. Liu, J. Song, Z. Zhao, S. Zhao, Z. Tian, and F. Yan, “Organic Electrochemical Transistors for Biomarker Detections,” *Advanced Science*, vol. 11, no. 27, Jul. 2024, doi: 10.1002/advs.202305347.

[15] F. Mahmud, A. Bello, P. Vijayrania, A. Kumar, and V. Budhraja, “An Electron Devices Perspective on the Technology Road Map for Implanted Electronics: A Review,” *IEEE Electron Devices Magazine*, vol. 4, no. 2, pp. 22–28, Jun. 2026, doi: 10.1109/MED.2026.3706522.

[16] D. A. Bernards, D. J. Macaya, M. Nikolou, J. A. DeFranco, S. Takamatsu, and G. G. Malliaras, “Enzymatic sensing with organic electrochemical transistors,” *J. Mater. Chem.*, vol. 18, no. 1, pp. 116–120, 2008, doi: 10.1039/B713122D.

[17] M. Sessolo, J. Rivnay, E. Bandiello, G. G. Malliaras, and H. J. Bolink, “Ion-Selective Organic Electrochemical Transistors,” *Advanced Materials*, vol. 26, no. 28, pp. 4803–4807, Jul. 2014, doi: 10.1002/adma.201400731.

[18] N. Coppedè *et al.*, “Ion selective textile organic electrochemical transistor for wearable sweat monitoring,” *Org. Electron.*, vol. 78, p. 105579, Mar. 2020, doi: 10.1016/j.orgel.2019.105579.

[19] X. Meng *et al.*, “Selective Ion Sensing Organic Electrochemical Transistors Suitable for Blood Analysis,” *Advanced Sensor Research*, vol. 3, no. 1, Jan. 2024, doi: 10.1002/adsr.202300097.

[20] C. Li, Z. Li, T. D. D. Nguyen, S. Ingebrandt, and X. T. Vu, “Real-time and multiplexed detection of sodium and potassium ions using PEDOT:PSS OECT microarrays integrated with ion-selective membranes,” *Electrochim. Acta*, vol. 507, p. 145111, Dec. 2024, doi: 10.1016/j.electacta.2024.145111.

[21] G. Frusconi, Z. M. Kovács-Vajna, and F. Torricelli, “Selective and Real-Time Ion Monitoring with Integrated Floating-Gate Organic Electrochemical Transistor Sensing Circuits,” *Adv. Mater. Technol.*, vol. 9, no. 19, Oct. 2024, doi: 10.1002/admt.202400301.

[22] A. Dasca Beneito *et al.*, “A Paper-Based Ion-Selective Organic Electrochemical Transistor for Highly Sensitive Determination of Creatinine and Potassium,” *ACS Omega*, vol. 10, no. 32, pp. 36475–36480, Aug. 2025, doi: 10.1021/acsomega.5c04973.

[23] E. J. Strand *et al.*, “Printed Organic Electrochemical Transistors for Detecting Nutrients in Whole Plant Sap,” *Adv. Electron. Mater.*, vol. 8, no. 4, Apr. 2022, doi: 10.1002/aelm.202100853.

[24] C. Li, S. Chen, C. Liu, H.-J. Chen, and S. Han, “A Flexible Multi-Ion Detection System Based on Organic Electrochemical Transistors for Physiological Monitoring,” *Electronics (Basel).*, vol. 14, no. 5, p. 1023, Mar. 2025, doi: 10.3390/electronics14051023.

[25] V. Budhraja, B. Khan, and A. S. Mehta, “Investigation of Electrochemical Transport, Gate Leakage, and Transconductance Behavior in PEDOT:PSS Organic Electrochemical Transistors,” *ECS Journal of Solid State Science and Technology*, vol. 15, no. 6, p. 067001, Jun. 2026, doi: 10.1149/2162-8777/ae7642.

[26] M. Tintelott, T. Kremers, S. Ingebrandt, V. Pachauri, and X. T. Vu, “Realization of a PEDOT:PSS/Graphene Oxide On-Chip Pseudo-Reference Electrode for Integrated ISFETs,” *Sensors*, vol. 22, no. 8, p. 2999, Apr. 2022, doi: 10.3390/s22082999.

[27] D. Alemu Mengistie, P.-C. Wang, and C.-W. Chu, “Effect of molecular weight of additives on the conductivity of PEDOT:PSS and efficiency for ITO-free organic solar cells,” *J. Mater. Chem. A Mater.*, vol. 1, no. 34, p. 9907, 2013, doi: 10.1039/c3ta11726j.

[28] J. L. Carter, C. A. Kelly, and M. J. Jenkins, “Processing optimization of PEDOT:PSS and PEDOT:PSS/Tween 80 films,” *Polym. J.*, vol. 55, no. 3, pp. 253–260, Mar. 2023, doi: 10.1038/s41428-022-00740-x.

[29] G. D. Spyropoulos, J. N. Gelinas, and D. Khodagholy, “Internal ion-gated organic electrochemical transistor: A building block for integrated bioelectronics,” *Sci. Adv.*, vol. 5, no. 2, Feb. 2019, doi: 10.1126/sciadv.aau7378.

[30] B. Friedel *et al.*, “Effects of Layer Thickness and Annealing of PEDOT:PSS Layers in Organic Photodetectors,” *Macromolecules*, vol. 42, no. 17, pp. 6741–6747, Sep. 2009, doi: 10.1021/ma901182u.

[31] H. Shi, C. Liu, Q. Jiang, and J. Xu, “Effective Approaches to Improve the Electrical Conductivity of PEDOT:PSS: A Review,” *Adv. Electron. Mater.*, vol. 1, no. 4, Apr. 2015, doi: 10.1002/aelm.201500017.

[32] D. Ohayon, V. Druet, and S. Inal, “A guide for the characterization of organic electrochemical transistors and channel materials,” *Chem. Soc. Rev.*, vol. 52, no. 3, pp. 1001–1023, 2023, doi: 10.1039/D2CS00920J.

[33] M. Luginieski, B. B. M. Torres, and G. C. Faria, “Guidelines on Measuring Volumetric Capacitance in Organic Electrochemical Transistors,” *ACS Appl. Electron. Mater.*, vol. 6, no. 4, pp. 2225–2231, Apr. 2024, doi: 10.1021/acsaelm.3c01673.

[34] S. Pecqueur, I. Lončarić, V. Zlatić, D. Vuillaume, and Ž. Crljen, “The non-ideal organic electrochemical transistors impedance,” *Org. Electron.*, vol. 71, pp. 14–23, Aug. 2019, doi: 10.1016/j.orgel.2019.05.001.

[35] D. Arcangeli *et al.*, “Potentiometric Detection of Calcium Ions Using an Organic Electrochemical Transistor,” *ACS Omega*, vol. 10, no. 29, pp. 32202–32215, Jul. 2025, doi: 10.1021/acsomega.5c03720.

[36] X. Meng *et al.*, “Selective Ion Sensing Organic Electrochemical Transistors Suitable for Blood Analysis,” *Advanced Sensor Research*, vol. 3, no. 1, Jan. 2024, doi: 10.1002/adsr.202300097.

[37] D. A. Bernards, D. J. Macaya, M. Nikolou, J. A. DeFranco, S. Takamatsu, and G. G. Malliaras, “Enzymatic sensing with organic electrochemical transistors,” *J. Mater. Chem.*, vol. 18, no. 1, pp. 116–120, 2008, doi: 10.1039/B713122D.

[38] J. T. Friedlein, R. R. McLeod, and J. Rivnay, “Device physics of organic electrochemical transistors,” *Org. Electron.*, vol. 63, pp. 398–414, Dec. 2018, doi: 10.1016/j.orgel.2018.09.010.

[39] A. J. . Bard, L. R. . Faulkner, and H. S. . White, *Electrochemical methods : fundamentals and applications*. John Wiley & Sons, Ltd., 2022.

[40] J. T. Friedlein *et al.*, “Influence of disorder on transfer characteristics of organic electrochemical transistors,” *Appl. Phys. Lett.*, vol. 111, no. 2, Jul. 2017, doi: 10.1063/1.4993776.

[41] J. T. Friedlein, M. J. Donahue, S. E. Shaheen, G. G. Malliaras, and R. R. McLeod, “Microsecond Response in Organic Electrochemical Transistors: Exceeding the Ionic Speed Limit,” *Advanced Materials*, vol. 28, no. 38, pp. 8398–8404, Oct. 2016, doi: 10.1002/adma.201602684.

[42] X. Tian *et al.*, “Pushing OECTs toward Wearable: Development of a Miniaturized Analytical Control Unit for Wireless Device Characterization,” *Anal. Chem.*, vol. 94, no. 16, pp. 6156–6162, Apr. 2022, doi: 10.1021/acs.analchem.1c05210.

[43] G. C. Faria, D. T. Duong, and A. Salleo, “On the transient response of organic electrochemical transistors,” *Org. Electron.*, vol. 45, pp. 215–221, Jun. 2017, doi: 10.1016/j.orgel.2017.03.021.

[44] S. T. M. Tan *et al.*, “Operation mechanism of organic electrochemical transistors as redox chemical transducers,” *J. Mater. Chem. C Mater.*, vol. 9, no. 36, pp. 12148–12158, 2021, doi: 10.1039/D1TC02224E.

[45] X. Ji *et al.*, “Highly Sensitive Metabolite Biosensor Based on Organic Electrochemical Transistor Integrated with Microfluidic Channel and Poly(N-vinyl-2-pyrrolidone)-Capped Platinum Nanoparticles,” *Adv. Mater. Technol.*, vol. 1, no. 5, Aug. 2016, doi: 10.1002/admt.201600042.

[46] A. W. Bevan, C.-L. Gee, M. Vermette, H. Kaur, S. Saghafifar, and L. G. Kaake, “Cyclic Voltammetry and Spectroelectrochemistry of Two Common Thiophene Polymers Reveals Ion Diffusion and Polaron Wave Function Extent,” *Chemistry of Materials*, vol. 37, no. 5, pp. 1949–1960, Mar. 2025, doi: 10.1021/acs.chemmater.4c03284.

[47] S. Yu and E. L. Ratcliff, “Tuning Organic Electrochemical Transistor (OECT) Transconductance toward Zero Gate Voltage in the Faradaic Mode,” *ACS Appl. Mater. Interfaces*, vol. 13, no. 42, pp. 50176–50186, Oct. 2021, doi: 10.1021/acsami.1c13009.

[48] D. Priyadarshini *et al.*, “Tuning the Organic Electrochemical Transistor (OECT) Threshold Voltage with Monomer Blends,” *Adv. Electron. Mater.*, vol. 11, no. 17, Oct. 2025, doi: 10.1002/aelm.202400681.

[49] C. Liao, C. Mak, M. Zhang, H. L. W. Chan, and F. Yan, “Flexible Organic Electrochemical Transistors for Highly Selective Enzyme Biosensors and Used for Saliva Testing,” *Advanced Materials*, vol. 27, no. 4, pp. 676–681, Jan. 2015, doi: 10.1002/adma.201404378.

[50] H.-R. Lim *et al.*, “Development of Flexible Ion-Selective Electrodes for Saliva Sodium Detection,” *Sensors*, vol. 21, no. 5, p. 1642, Feb. 2021, doi: 10.3390/s21051642.

[51] G. Kassahun *et al.*, “Polymerization-Charge Controlled Threshold Voltage Tunability in Organic Electrochemical Transistors,” *Adv. Electron. Mater.*, vol. 12, no. 1, Jan. 2026, doi: 10.1002/aelm.202500357.

[52] S. Inal, G. G. Malliaras, and J. Rivnay, “Benchmarking organic mixed conductors for transistors,” *Nat. Commun.*, vol. 8, no. 1, p. 1767, Nov. 2017, doi: 10.1038/s41467-017-01812-w.

[53] Y. Kim, J. Kimpel, A. Giovannitti, and C. Müller, “Small signal analysis for the characterization of organic electrochemical transistors,” *Nat. Commun.*, vol. 15, no. 1, p. 7606, Sep. 2024, doi: 10.1038/s41467-024-51883-9.

[54] G. E. Fenoy *et al.*, “Interface Engineering of ‘Clickable’ Organic Electrochemical Transistors toward Biosensing Devices,” *ACS Appl. Mater. Interfaces*, vol. 15, no. 8, pp. 10885–10896, Mar. 2023, doi: 10.1021/acsami.2c21493.

[55] A. V. Volkov *et al.*, “Understanding the Capacitance of PEDOT:PSS,” *Adv. Funct. Mater.*, vol. 27, no. 28, Jul. 2017, doi: 10.1002/adfm.201700329.

[56] G. E. Fenoy *et al.*, “‘Clickable’ Organic Electrochemical Transistors,” *JACS Au*, vol. 2, no. 12, pp. 2778–2790, Dec. 2022, doi: 10.1021/jacsau.2c00515.

[57] M. F. S. Teixeira, B. H. Freitas, P. M. Seraphim, L. O. Salmazo, M. A. Nobre, and S. Lanfredi, “Development of an electrochemical sensor for potassium ions based on KSr2Nb5O15 modified electrode,” *Procedia Chem.*, vol. 1, no. 1, pp. 293–296, Sep. 2009, doi: 10.1016/j.proche.2009.07.073.

[58] P. Pirovano *et al.*, “A wearable sensor for the detection of sodium and potassium in human sweat during exercise,” *Talanta*, vol. 219, p. 121145, Nov. 2020, doi: 10.1016/j.talanta.2020.121145.

[59] L. Ma, W. Hou, Z. Ji, Z. Sun, M. Li, and B. Lian, “Wearable Electrochemical Sensor for Sweat-Based Potassium Ion and Glucose Detection in Exercise Health Monitoring,” *ChemistryOpen*, vol. 13, no. 8, Aug. 2024, doi: 10.1002/open.202300217.

[60] F. Arshadi *et al.*, “A miniaturized electrochemical biosensor for real-time in vivo potassium monitoring in the inner ear,” *Biosens. Bioelectron.*, vol. 298, p. 118388, Apr. 2026, doi: 10.1016/j.bios.2026.118388.